2018 IEEE Intelligent Vehicles Symposium (IV)
Changshu, Suzhou, China, June 26-30, 2018

Pedestrian Classification for 79 GHz Automotive Radar Systems

Robert Prophet*, Marcel Hoffmann*, Alicja Ossowska†, Waqas Malik†, Christian Sturm†, and Martin Vossiek*
*Institute of Microwaves and Photonics (LHFT), Friedrich-Alexander-Universität Erlangen-Nürnberg, 91054 Erlangen, Germany
†Active Safety Product Line, VALEO Schalter und Sensoren GmbH, Bietigheim-Bissingen, Germany
Email: robert.prophet@fau.de

***Abstract*—Radar sensors have become an integral part of advanced driver assistance systems. Merely detecting targets will not, however, advance their contribution. Rather, an object classification capability is required to distinguish vulnerable road users from other objects, such as vehicles. To achieve this, targets that are determined from the range-Doppler-Matrix created by a 79 GHz chirp sequence radar are clustered to objects. Different classifiers then use previously calculated characteristic features of moving objects to generate the object classes "Pedestrian" and "Other". As a result, the success rate of one measurement reaches up to 95.3% for well-suited classifiers and a bandwidth of 1.6 GHz. Moreover, the robustness of the classification process is increased by tracking the objects. The proposed algorithm for pedestrian classification is not only faster than conventional approaches using micro-Doppler signatures, but also requires less computational effort. Implemented in vehicles, this can be a major contribution to protect vulnerable road users such as pedestrians.**

***Index Terms*—79 GHz, Automotive Radar, Chirp Sequence, Machine Learning, Pedestrian Classification**

I. Introduction

The all-weather capability, the accurate range and radial velocity measurements as well as the imaging capability make automotive radar sensors a strong candidate for several different advanced driver assistance systems (ADAS). Moreover, the small size of 79 GHz sensors and the possible installation behind the bumper facilitate the integration in future vehicles. Automotive radar sensors detect targets in the vehicle's immediate vicinity up to a maximum range of 200 m. Next generation radars even provide information on the elevation angle.

For a better scene understanding, a classification of the radar targets is essential. In this context, many classification algorithms are based on *micro-Doppler signatures*. [1] offers an extensive compilation in this field, which shows beneficial results concerning classifications of human and quadrupedal animal motions. However, the evaluation of micro-Doppler signatures requires a long observation time of up to a few seconds, which is a major drawback in the fast-paced urban traffic. In [2], S. Heuel deployed 24 GHz radar sensors and calculated certain features from a single measurement to distinguish walking pedestrians from longitudinally and laterally driving vehicles. This led to a profitable classification update rate of 25 Hz.

In this paper, we present a novel pedestrian classification procedure based on 79 GHz *chirp sequence* radar sensors. In contrast to other publications, we are not limited to a distinction between pedestrians and vehicles, but also consider cyclists and dogs. The paper is structured as follows: Section II gives an introduction of the used radar sensor and the basic processing steps. The actual classification procedure is presented in section III. After a discussion of the data collection and experimental results in section IV and V, a conclusion including a brief outlook for future work is given in section VI.

II. Preprocessing

The deployed radar sensor uses the fast chirp sequence waveform, which is described in [3]. One measurement cycle contains the coherent processing interval time T_{CPI}, which consists of N_{chirp} linear frequency modulated chirps each characterized by the duration T_{chirp}, the pause T_{pause} between two chirps, the bandwidth $B = f_{max} - f_{min}$, and N_{range} sample points. Thus, the signal's frequency varies over time between the maximum frequency f_{max} and the minimum frequency f_{min}, which is exemplarily shown in Fig. 1 for one measurement cycle. As a consequence, every measurement cycle provides N_{range} times N_{chirp} samples, which are typically stored in a 2D matrix with a slow time axis with multiples of the sum $T_{chirp} + T_{pause}$ and a fast time axis with multiples of the reciprocal sample frequency. On this basis, the following four consecutive steps are performed: *2D Fast Fourier Transformation*, *Target*

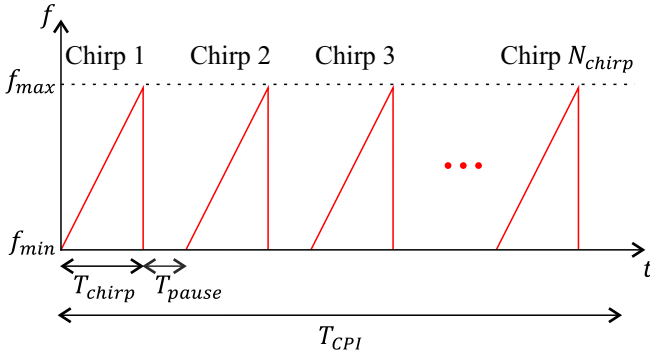

Fig. 1. Fast chirp sequence waveform of a single CPI.

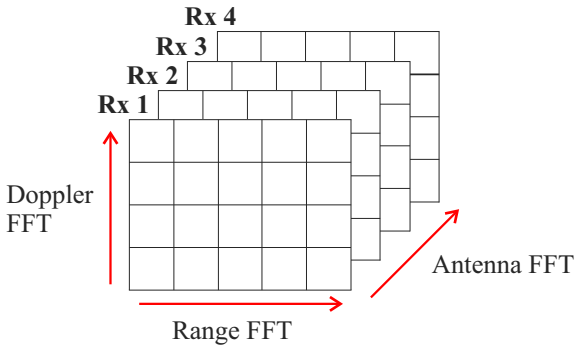

Fig. 2. Exemplary 3D radar data representation for four receiving antennas.

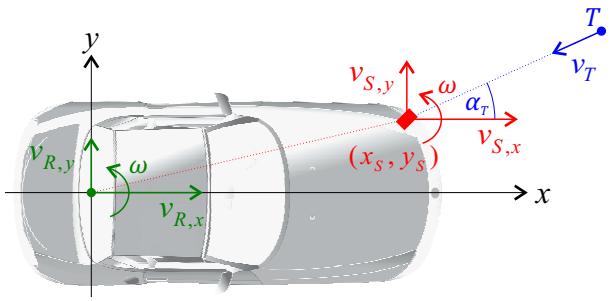

Fig. 3. The vehicle motion (green) specified at the reference point and the corresponding sensor motion in the front left (red). Its velocity vector is compared to the target's radial velocity vector (blue).

Detection, *Azimuth Angle Estimation*, and *Dynamic Target Identification*.

A. 2D Fast Fourier Transformation

The 2D time domain matrix is transformed to the 2D frequency domain matrix by means of a 2D fast Fourier transformation (FFT). As the frequencies are directly proportional to the range and the relative radial velocity of the detected target, this matrix is again transferred to the well-known *range-Doppler-Matrix* (RDM) with the range resolution

$$\Delta R = \frac{c}{2 \cdot B} \tag{1}$$

and the velocity resolution

$$\Delta v = \frac{c}{2 \cdot f_c \cdot T_{CPI}}, \tag{2}$$

where f_c denotes the chirp's center frequency and c the speed of light. The maximum range and velocity without ambiguity depends on the corresponding number of samples and amounts for the range to

$$R_{unamb} = \frac{N_{range}}{2} \cdot \Delta R \tag{3}$$

and for the velocity to

$$v_{unamb} = \pm \frac{N_{chirp}}{2} \cdot \Delta v\,. \tag{4}$$

To extend the velocity unambiguity, the coherent processing interval time T_{CPI} is changed periodically leading also to a change of the velocity resolution Δv. For a target velocity v_{target}, this will result in the congruences

$$v_{target} \equiv v_{T,CPI\,1} \bmod \left(2 \cdot v_{unamb,CPI\,1}\right), \tag{5}$$

$$v_{target} \equiv v_{T,CPI\,2} \bmod \left(2 \cdot v_{unamb,CPI\,2}\right). \tag{6}$$

From the measured velocity of the target $v_{T,CPI\,1}$ respectively $v_{T,CPI\,2}$ with the velocity unambiguity $2 \cdot v_{unamb,CPI\,1}$ respectively $2 \cdot v_{unamb,CPI\,2}$, the target's velocity $v_{T,comb}$ can be calculated with a significantly larger velocity unambiguity, which equals the least common multiple of $2 \cdot v_{unamb,CPI\,1}$ and $2 \cdot v_{unamb,CPI\,2}$. A more detailed description including derivations is given in [4].

B. Target Detection

Targets appear as local maxima above a certain threshold inside the RDM. As the noise level is not constant over the frequency. Therefore, a constant threshold will lead to non-constant target detections that is, non-constant false alarms. Instead, we use an algorithm presented in [5] as a fast 2D Constant False Alarm Rate (CFAR) procedure called *Fast Ordered Statistics Cell Averaging CFAR* (FOSCACFAR). This algorithm applies an OSCFAR along the range dimension and a CACFAR along the velocity dimension. Furthermore, the OSCFAR is only performed for a fraction of the range rows of the RDM to reduce computational effort. Interpolating the skipped range rows degrades the outcome only slightly. Hence, the local RDM maxima exceeding the values of the corresponding cells in the calculated threshold matrix are declared as targets.

C. Azimuth Angle Estimation

A multiple antenna array is used for the azimuth angle estimation for each target. As one of several possible methods, we calculate a third FFT along the antenna array as a part of digital beamforming. With $N_{antenna}$ receiving antennas, the total sample number for one measurement cycle is equal to $N_{range} \cdot N_{chirp} \cdot N_{antenna}$. Fig. 2 displays the so-called data cube. With known target distance and azimuth, it becomes possible to create a 2D representation of the environment, e.g. a radar based *occupancy gridmap*.

D. Dynamic Target Identification

Scene understanding is greatly improved by identifying non-stationary targets (aka dynamic targets). With access to the vehicle's odometry data, this task is reduced to a simple comparison of the projected sensor velocity and the relative radial target velocity. Fig. 3 depicts an example. With the known 2D motion vector $\boldsymbol{s}_R = \left(\omega, v_{R,x}, v_{R,y}\right)^T$ of the reference point being typically the middle of the rear axle as well as the mounting position (x_S, y_S) of the sensor, the sensor's 2D motion vector $\boldsymbol{s}_S = \left(\omega, v_{S,x}, v_{S,y}\right)^T$ equals

$$\boldsymbol{s}_S = \boldsymbol{s}_R + \begin{pmatrix} 0 \\ -\omega \cdot y_S \\ \omega \cdot x_S \end{pmatrix} = \begin{pmatrix} \omega \\ v_{R,x} - \omega \cdot y_S \\ v_{R,y} + \omega \cdot x_S \end{pmatrix}. \tag{7}$$

The target T, which has the measured azimuth α_T and the measured radial velocity component v_T, is *static* regarding the radial velocity component, iff equation (8) is fulfilled:

$$-v_T = \cos(\alpha_T) \cdot v_{S,x} + \sin(\alpha_T) \cdot v_{S,y}\,. \tag{8}$$

Otherwise, T is *dynamic*. In the seldom case of a pure tangential motion, T is also dynamic despite the satisfied equation (8).

The authors in [6] showed that the identification of dynamic targets is even possible without any odometry data. For this, the azimuth-velocity space is investigated. All static targets lie on a sine function, while dynamic targets deviate from this curve due to their ego motion. Assuming that most targets are static, these targets can be identified by means of a *Random Sample Consensus* (RANSAC) algorithm. However, the result of this procedure greatly depends on the velocity and azimuth accuracy.

III. Algorithm Chain

The proposed algorithm consists of four consecutive steps: *Clustering*, *Feature Calculation*, *Classification*, and *Tracking*. The first three steps lead to a classification result of a single measurement cycle, while the last one combines all previous classification results in order to filter wrong classifications.

A. Clustering

In this step, targets belonging to the same extended moving object are marked with the same label and build a cluster. Many different clustering algorithms are covered in the literature. As hierarchical clustering algorithms require a-priori knowledge of the number of clusters, which is not given in most cases, we use the *Density Based Spatial Clustering for Applications with Noise* (DBSCAN) algorithm. This algorithm was first described in [7] and adapted for automotive radar scenarios by the authors of [8]. In short, DBSCAN defines a target as a so-called core point, when it has at least $MinPts$ other targets within the distance ε. Neighboring core points, which are reachable over ε to each other, form a cluster. Furthermore, the targets belong to this cluster, which are not core points itself but reachable over ε to core points. Targets, which are neither core points nor reachable in that way represent noise points. In our algorithm, we set $MinPts = 2$ and $\varepsilon = 1$ m in contrast to [8], where an additional $\varepsilon_{vel} = 1\frac{\mathrm{m}}{\mathrm{s}}$ is used in the velocity dimension. Especially in the case of a walking pedestrian, this value may become critical, since the difference between the respective velocities of a fixed and swinging foot tends to be large.

B. Feature Calculation

To distinguish different kinds of moving objects, several features have to be defined and calculated. Based on [2], the authors in [9] introduce an extensive feature set being the basis for our approach. However, we implement two important differences:

1. According to [9] the value of the variable κ is a feature representing the error in the equation system

$$\begin{pmatrix} v_{T,1} \\ v_{T,2} \\ \vdots \\ v_{T,N} \end{pmatrix} = \begin{pmatrix} \cos(\alpha_{T,1}) & \sin(\alpha_{T,1}) \\ \cos(\alpha_{T,2}) & \sin(\alpha_{T,2}) \\ \vdots & \vdots \\ \cos(\alpha_{T,N}) & \sin(\alpha_{T,N}) \end{pmatrix} \cdot \begin{pmatrix} v_{S\,rel,x} \\ v_{S\,rel,y} \end{pmatrix}. \quad (9)$$

   This equation system corresponds to the approach in [6] and is used for a calculation of the vectorial velocity of the object. This calculation is based on the determination of the relative velocity $\boldsymbol{v}_{S\,rel} = \left(v_{S\,rel,x}, v_{S\,rel,y}\right)^T$ between the radar sensor and the moving object. Therefore, $N \geq 2$ targets with the azimuth angles $\alpha_{T,i}$ and radial velocities $v_{T,i}$ are required with $i = 1, \ldots, N$. Obviously, (9) is over-determined for $N > 2$ so that a minimum mean square estimation is performed to calculate $\boldsymbol{v}_{S\,rel}$. The idea in [9] is that solid bodies like vehicles supply a well-conditioned equation system respectively a low κ, whereas pedestrians supply a bad-conditioned equation system respectively a high κ due to their different motions of arms and legs. However, in case of $N = 2$, which occurs frequently for low range resolutions, *every* object leads to $\kappa = 0$. For this reason, we omit this feature.

2. We add the feature $\sum \Delta x, \Delta y$ representing the sum of the object's size in x- and y-direction within the 2D representation. Assuming perfect detection and clustering, the object size is obviously a great feature to distinguish a vehicle from a pedestrian.

Table I. Feature set

Feature	Description
Δv	Velocity Resolution
$N_{targets}$	Number of targets
ST	Existence of a static target
$\bar{\alpha}$	Mean of directions of arrival
$\bar{R}$	Mean of ranges
$\bar{P}$	Mean of normalized reflected powers
$\sum \Delta x, \Delta y$	Sum of object's size in x- and y-direction
$R_{profile}$	Extension in range
R_2	Variance estimation in range
R_3	Deviation estimation in range
$v_{profile}$	Extension in radial velocity
v_2	Variance estimation in radial velocity
v_3	Deviation estimation in radial velocity

Table I contains the complete feature set. As we do not create different classifiers for different velocity resolutions Δv, compare section II A, we take this variable as an additional feature. Concerning the last six features, a more detailed description is given in [2] and [9].

C. Classification

The assignment of a cluster representing a moving object to a class is performed by a decision algorithm, which takes the aforementioned features as input. This process is the actual classification. In terms of *supervised* classifiers, the parameters of the classifier are generated in a training phase by using a training data set, in which the class of the given cluster is always known. The verification of the found parameters is performed in an evaluation phase with a test data set. In this paper, we want to distinguish between the two classes *Pedestrian* and *Other*.

A widely used classifier based on statistical learning theory respectively machine learning is the *support vector machine* (SVM), which was introduced by Boser et al. in [10] in 1992. There are different kinds of SVMs, such as linear, quadratic, or cubic SVMs, differing in their calculated hyperplanes, to separate the hyperspace corresponding to the different classes. Besides the SVM, other common machine learning classifiers, like *decision trees*, *nearest neighbor*

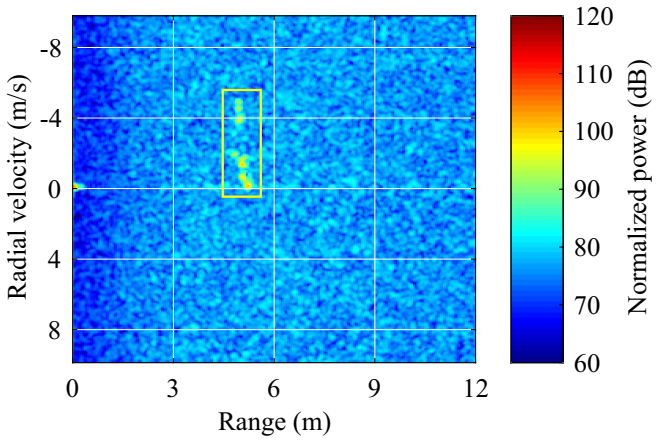

(a) RDM. With the high-resolution radar from Valeo, the individual body parts can be separated in both dimensions.

(b) Ground truth.

Fig. 4. Radially walking pedestrian with $v = 1.5\,\frac{\mathrm{m}}{\mathrm{s}}$ measured with 1.6 GHz.

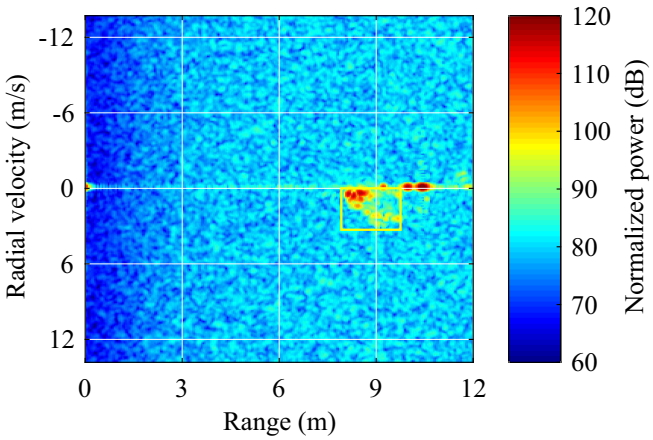

(a) RDM. The velocity of the reflection is significantly lower than the velocity of the center of gravity due to its lateral motion. The infrastructure creates reflections outside the magenta rectangle.

(b) Ground truth.

Fig. 5. Laterally driving vehicle with $v = 8\,\frac{\mathrm{m}}{\mathrm{s}}$ measured with 1.6 GHz.

classifiers (KNN), and *neural networks (NN)*, yield good results as well.

D. Tracking

As wrong classifications may occur in a single measurement cycle, a merged result of classifications of consecutive measurement cycles will be more robust. The moving object is tracked for this purpose. With high resolution radar systems, this can be achieved with a nearest neighbor algorithm, which associates the object's cluster in measurement cycle t with the cluster for the same object in cycle $t+1$. The merged classification result can be calculated by simply adding up the individual classification results.

IV. Data Collection

To collect the necessary training data, several measurements were conducted with a 79 GHz radar sensor prototype from Valeo. The sensor employs the described chirp sequence waveform, and features four receiving channels; it has an angular accuracy of better than 1° over the complete field of view. The sensor can run two bandwidths: $B_1 = 0.4\,\mathrm{GHz}$ and $B_2 = 1.6\,\mathrm{GHz}$. Hence, the range resolution varies between 37.5 cm and 9.375 cm. As a fixed number of samples in range $N_{range} = 512$ is used, the maximum unambiguous distance is either 96 m or 24 m. Because range resolution difference is relatively high, we conducted measurements with both bandwidths, creating a separate classifier for each bandwidth. As mentioned before, we want to assign the objects' clusters to the Pedestrian and Other classes. Regarding the latter class, we consider vehicles, cyclists, and dogs, whose characteristic RDM signatures are discussed in the following.

A. Pedestrians

Within the RDM, a pedestrian yields a significantly higher extension in the Doppler dimension than in the range dimension. This follows from their fixed foot with a very small velocity component and their swinging foot being up to three times faster than the torso (compare [1]), whereas the radial distance between the feet is usually not greater than 1.5 m. However, these relations greatly depend on the pedestrian's walking direction relative to the sensor as well as their mean velocity: The more lateral the movement or the slower the gait, the smaller the extensions of the pedestrian in both range and Doppler dimension. Fig. 4 displays a radially walking pedestrian.

B. Vehicles

A significant difference between pedestrians and vehicles is the reflected power due to a vehicle's distinct radar cross section (RCS). Furthermore, its extension is higher inside the RDM leading to an increased number of targets, which are usually distributed at greater distances to each other, because the RCS varies more over the vehicle body than with pedestrians. The velocity components of the vehicle body are equal in the case of non-rotational motion. However, the reflections of the rotating tires generate targets with a velocity between zero and twice the velocity of the center of gravity. This circumstance may impede a usage of the feature κ too, which was discussed in section III B. Fig. 5 pictures a laterally driving vehicle.

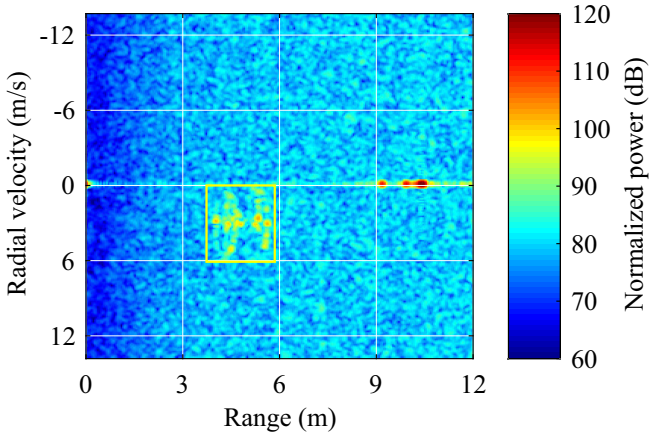

(a) RDM. The range extension of 1.8 m and the velocity extension of $6\frac{\text{m}}{\text{s}}$ differ slightly from the ground truth, because the motion is not exactly radial.

(b) Ground truth.

Fig. 6. Radially moving cyclist with $v = 4\frac{\text{m}}{\text{s}}$ measured with 1.6 GHz.

C. Cyclists

The RDM signature of a cyclist was intensively investigated in [11]. Due to the rotating wheels with many spokes, as for vehicles the effect of the large velocity extension is more marked, since there are always several spokes orthogonal to the radar waves. This is also one reason why the reflected power is higher than with humans. Fig. 6 depicts a radially moving cyclist.

D. Dogs

Currently, there are only a few investigations on dogs or quadrupedal animals in general with automotive radar systems. Most dogs are significantly smaller in height than humans, but they can be larger in the horizontal dimension. This influences their RDM signature in two ways: Firstly, they have a larger extension in range compared to humans, which usually results in a higher number of targets. Secondly, their reflected power is slightly lower. Additionally, they exhibit a different velocity profile due to their two extra legs. Fig. 7 displays a laterally running dog.

V. Experimental Results

The data sets used in our trials consist of 8500 clusters of each of the Pedestrian and Other classes for B_2, and 2600 clusters of each class for B_1. These data sets are split in 85% training and 15% test data sets for each bandwidth. To demonstrate the effect of the developed algorithms, the results of the single measurement classifications for the test data sets are shown in Table II and III as confusion matrices. These results were achieved for the respective best

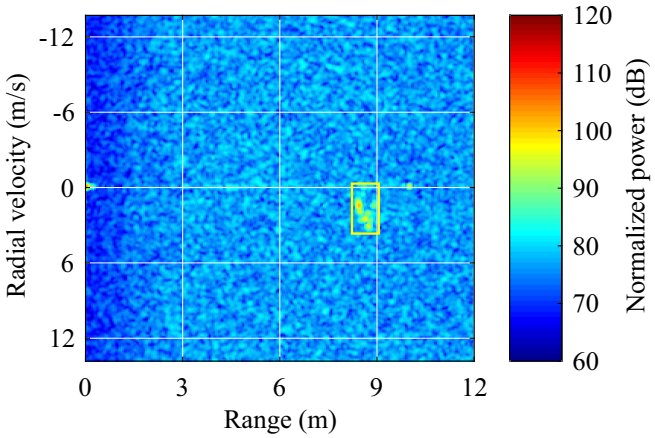

(a) RDM. The extension in velocity is smaller than in Fig. 4 (a) due to the lateral movement. In the case of a more radial movement, dogs create significantly higher velocity extensions than humans.

(b) Ground truth.

Fig. 7. Laterally running dog weighing 18 kg with $v = 5\frac{\text{m}}{\text{s}}$ measured with 1.6 GHz.

Table II. Confusion matrix of the best single measurement classification results for $B_2 = 1.6$ GHz

		Actual class: Pedestrian	Actual class: Other
Predicted class	Pedestrian	95.0%	5.0%
	Other	4.3%	95.7%

Table III. Confusion matrix of the best single measurement classification results for $B_1 = 0.4$ GHz

		Actual class: Pedestrian	Actual class: Other
Predicted class	Pedestrian	93.5%	6.5%
	Other	4.7%	95.3%

classifiers. Furthermore, Table IV and V give an overview of the results of the individual classifiers.

For both bandwidths, the best classifiers show good performances. The classification process will be even better, if the moving object is tracked so that wrong classifications can be filtered. As the Valeo radar has a cycle time of 50 ms, this procedure is relatively fast. However, the performance strongly depends on the chosen classifier: E.g., the simple

decision tree leads to a significantly worse result of merely 81.7% respectively 86.9% compared to the ensemble bagged trees classifier, which combines the results of various classifiers. On the other side, such ensemble classifiers require an increased amount of memory of typically more than 100 MB. Thus, an implementation on an embedded system may become challenging. A good compromise between performance and memory requirement represent our fully connected NN with only one hidden layer, which achieved a success rate of 92.9 % respectively 93.2 % with only 3 kB memory.

The classification process is not only affected by the classification itself, but also by the previous clustering. In our experiments, vehicles were frequently split into more than one cluster, because the chosen ε in the DBSCAN algorithm is too small for these objects. However, a bigger ε would lead to extended clusters, which may include infrastructure targets especially in the case of a pedestrian walking next to a wall. In general, target clustering is still a main issue for automotive radar systems. Besides better range and angular resolutions, clustering based on machine learning is also possible.

VI. Conclusion

In this paper, an algorithm to classify pedestrians based on machine learning is presented. The algorithm evaluates the RDM, which is gained from the time signal of a chirp sequence automotive radar. As a first step, detected targets are clustered by DBSCAN in order to identify targets belonging to the same moving object. Subsequently, characteristic features are calculated and used as input for the actual classifier, which divides the clusters into the classes Pedestrian and Other. To make the classification result more robust, a nearest neighbor based tracking algorithm is performed, which combines the classification results of individual measurement cycles. As a result, the best classifiers achieve success rates of approximately 95 % for a single measurement for both used bandwidths respectively range resolutions. As a measurement cycle requires 50 ms, the procedure is significantly faster than a micro-Doppler based pedestrian classification.

The proposed algorithm brings autonomously driving cars closer to the important milestone, where radar sensors are not only deployed for detection and ranging. Instead, they can more actively and on a higher level contribute to the vehicle's decision making and to the optimization of the path finding process. When vulnerable road users and thereby their class-specific behavior can reliably and successfully be identified, the vehicle is able to drive more intelligent, better-adjusted to the current traffic and, overall, safer. The further evaluation of class-specific behavior is a task for future work, which also has to determine extended classifiers that split clustered objects of the class Other into individual classes.

Table IV. Single measurement success rates for various classifiers for $B_2 = 1.6$ GHz

Classifier	Probability of success
Simple decision tree	81.7%
Complex decision tree	92.1%
Linear SVM	86.3%
Quadratic SVM	91.8%
Cubic SVM	93.1%
Fine Gaussian SVM	93.8%
Coarse Gaussian SVM	89.0%
Fine KNN	93.0%
Medium KNN	92.9%
Coarse KNN	89.9%
Cosine KNN	92.8%
Ensemble subspace KNN	94.8%
Ensemble bagged trees	95.3%
Fully connected NN	92.9%

Table V. Single measurement success rates for various classifiers for $B_1 = 0.4$ GHz

Classifier	Probability of success
Simple decision tree	86.9%
Complex decision tree	92.6%
Linear SVM	87.5%
Quadratic SVM	90.8%
Cubic SVM	91.9%
Fine Gaussian SVM	90.4%
Coarse Gaussian SVM	88.6%
Fine KNN	89.8%
Medium KNN	91.2%
Coarse KNN	87.6%
Cosine KNN	90.7%
Ensemble subspace KNN	94.1%
Ensemble bagged trees	94.4%
Fully connected NN	93.2%

References

[1] D. Tahmoush, "Review of micro-Doppler signatures", in *2015 IET Radar, Sonar & Navigation*, December 2015, pp. 1140-1146.

[2] S. Heuel, H. Rohling, "Pedestrian classification in automotive radar systems", in *Radar Symposium (IRS)*, May 2012.

[3] M. Mandlik, C. Sturm, U. Lübbert, T. Vajdiak, J. Kubak, "Multiband Automotive Radar Sensor with Agile Bandwidth", in *2017 IEEE-APS Topical Conference on Antennas and Propagation in Wireless Communications (APWC)*, September 2017, pp. 163-165.

[4] A. Wojtkiewicz et al., "Two-dimensional signal processing in FMCW radars", in *XXth National Conference on Circuit Theory and Electronic Networks*, October 1997.

[5] M. Kronauge, H. Rohling, "Fast Two-Dimensional CFAR Procedure", in *IEEE Transactions on Aerospace and Electronic Systems*, July 2013, pp. 1817-1823.

[6] D. Kellner, M. Barjenbruch, J. Klappstein, J. Dickmann, K. Dietmayer, "Instantaneous Ego-Motion Estimation using Multiple Doppler Radars" in *Robotics and Automation (ICRA)*, June 2014.

[7] M. Ester, H.-P. Kriegel, J. Sander, X. Xu, "A Density-Based Algorithm for Discovering Clusters in Large Spatial Databases with Noise", in *Proceedings of the Second International Conference on Knowledge Discovery and Data Mining*, August 1996, pp. 226-231.

[8] E. Schubert et al., "Clustering of High Resolution Automotive Radar Detections and Subsequent Feature Extraction for Classification of Road Users", in *Radar Symposium (IRS)*, August 2015.

[9] S. Heuel, "Fußgängererkennung im Straßenverkehr mit 24 GHz Radarsensoren", doctoral thesis, 2013.

[10] B. E. Boser, I. M. Guyon, V. N. Vapnik, "A training algorithm for optimal margin classifiers", in *5th Annual ACM Workshop on COLT*, 1992, pp. 144-152.

[11] M. Stolz, E. Schubert, F. Meinl, M. Kunert, W. Menzel, "Multi-Target Reflection Point Model of Cyclists for Automotive Radar", in *European Radar Conference (EURAD)*, October 2017, pp. 94-97.